MCB
Journals.ASM.org

New Insights into Structural Determinants for Prostanoid Thromboxane A2 Receptor- and Prostacyclin Receptor-G Protein Coupling

Raja Chakraborty,[a] Sai Prasad Pydi,[a] Scott Gleim,[d] Rajinder Pal Bhullar,[a] John Hwa,[d] Shyamala Dakshinamurti,[b,c] Prashen Chelikani[a,c]

Department of Oral Biology, University of Manitoba, Winnipeg, Manitoba, Canada[a]; Departments of Pediatrics and Physiology, University of Manitoba, Winnipeg, Manitoba, Canada[b]; Manitoba Institute of Child Health, Winnipeg, Manitoba, Canada[c]; Department of Internal Medicine (Cardiology), Cardiovascular Research Center, Yale University School of Medicine, New Haven, Connecticut, USA[d]

G protein-coupled receptors (GPCRs) interact with heterotrimeric G proteins and initiate a wide variety of signaling pathways. The molecular nature of GPCR-G protein interactions in the clinically important thromboxane A2 (TxA_2) receptor (TP) and prostacyclin (PGI_2) receptor (IP) is poorly understood. The TP activates its cognate G protein (Gαq) in response to the binding of thromboxane, while the IP signals through Gαs in response to the binding of prostacyclin. Here, we utilized a combination of approaches consisting of chimeric receptors, molecular modeling, and site-directed mutagenesis to precisely study the specificity of G protein coupling. Multiple chimeric receptors were constructed by replacing the TP intracellular loops (ICLs) with the ICL regions of the IP. Our results demonstrate that both the sequences and lengths of ICL2 and ICL3 influenced G protein specificity. Importantly, we identified a precise ICL region on the prostanoid receptors TP and IP that can switch G protein specificities. The validities of the chimeric technique and the derived molecular model were confirmed by introducing clinically relevant naturally occurring mutations (R60L in the TP and R212C in the IP). Our findings provide new molecular insights into prostanoid receptor-G protein interactions, which are of general significance for understanding the structural basis of G protein activation by GPCRs in basic health and cardiovascular disease.

G protein-coupled receptors (GPCRs) contain seven transmembrane (TM) helices and signal predominantly through heterotrimeric G proteins in response to diverse extracellular stimuli, including neurotransmitters, light, taste, and smell. GPCRs form the largest group of membrane receptors and are divided into four classes, with the pharmacologically important class A comprising more than 70% of the GPCRs present in humans (1). The prostanoid receptors belong to the class A GPCR family and are poorly characterized in their structural aspects. The prostanoids thromboxane A2 (TxA_2) and prostacyclin (PGI_2) have been shown to play crucial but opposing vascular roles, with TxA_2 stimulating platelet aggregation and vasoconstriction and PGI_2 inhibiting platelet aggregation and causing vasodilation (2–4). The recent withdrawal of selective cyclooxygenase 2 (COX-2) inhibitors (e.g., Vioxx) due to increased numbers of cardiovascular events (5) and cardiovascular concerns with nonsteroidal anti-inflammatory drugs (NSAIDs) (e.g., ibuprofen) (6, 7) highlight the importance of understanding the G protein specificity of these opposing receptors. The thromboxane A2 receptor (TP) activates its cognate G protein (Gαq) in response to binding to TxA_2, while the prostacyclin receptor (IP) mediates signaling in response to the binding of PGI_2, primarily through the Gαs-based effector system. In addition, previous studies have shown that the IP is capable of coupling to multiple G proteins in a species- and/or tissue-specific manner, although the molecular basis behind this coupling to different G proteins is not properly understood (8–10).

The activation of a GPCR leads to structural protein changes in the cytoplasmic loops to activate the G protein. The recent structural elucidation of the metarhodopsin II bound to a peptide (11) and the β_2-adrenergic receptor (β_2AR)-Gs (the stimulatory protein for adenylyl cyclase) protein complex (12) give new insights into how GPCR-G protein complex formation occurs. These two structures now set the stage to identify sequence and structural features on GPCRs that may define specificities for particular G proteins.

In the prostanoid receptor subfamily, there is limited structural and functional information on the role of intracellular loops (ICLs) in the binding and activation of G proteins. Previous site-directed mutagenesis studies on the TP hypothesized that all three ICL regions are involved in determining G protein selectivity and specificity (13–15). The dominantly inherited bleeding disorder variant R60L in ICL1, the F138D mutation in ICL2, and the C223S mutation at the TM5/ICL3 boundary affected agonist-induced calcium signaling (16, 17).

In this study, by using a chimeric receptor approach combined with molecular modeling and site-directed mutagenesis, we analyzed the role of ICL regions among the prostanoid receptors TP and IP that determine the binding and activation of Gαq and Gαs, respectively. We systematically replaced each of the three TP ICL regions with the ICL regions of the IP. In the case of larger ICLs, such as ICL2 and ICL3, multiple chimeras were required in order to determine the minimal structural region of the loop that is

Received 30 May 2012 Returned for modification 13 July 2012
Accepted 23 October 2012
Published ahead of print 29 October 2012
Address correspondence to Prashen Chelikani, chelikan@cc.umanitoba.ca.
Supplemental material for this article may be found at http://dx.doi.org/10.1128/MCB.00725-12.

doi:10.1128/MCB.00725-12

required for optimal G protein coupling and signaling. Therefore, sequential replacement of the ICL2 and ICL3 of the TP with those of the IP was also pursued. In these replacements, the amino acid sequences and lengths of ICL2 and ICL3 influenced G protein activation, receptor folding, and the level of constitutive activity. To elucidate the structural constraints in the loops of each of the chimeric receptors that might be responsible for the observed activities, molecular modeling studies were pursued on the chimeric receptors that are bound to a C-terminal peptide fragment of the Gα subunit. The most interesting chimeric receptor is TP ICL2B-3B–IP; with an intermediate number of TP ICL2 and TP ICL3 amino acids replaced by IP ICL2 and IP ICL3, it showed TP agonist U46619-induced cyclic AMP (cAMP) accumulation of up to 90% of the wild-type (WT) IP induced with iloprost and Gαq-mediated inositol-1,4,5-trisphosphate (IP_3) and Ca^{2+} signaling of up to 90% of the wild-type TP. Next, to validate our molecular models, site-specific mutations were constructed. To test the stringency of our chimeric constructs, we introduced naturally occurring mutations present in the ICL regions into select chimeras. The TP ICL2B-3B–IP chimera was able to rescue the signaling of the dysfunctional genetic variant R60L to that of wild-type TP levels. Our results show that the predominant ICLs that determine G protein specificities among the prostanoid receptors are ICL2 and ICL3. We discuss our findings in the context of the recent structures of GPCR-G protein complexes.

MATERIALS AND METHODS

The TP antagonist ^{3}H-labeled SQ 29548 was purchased from PerkinElmer (product no. NET936250UC). The TP agonist U46619 and the IP agonist iloprost were purchased from the Cayman Chemicals Company (Michigan). Protease inhibitors and common chemicals were purchased from either Fisher or Sigma. The buffers and detergents were the same as those used previously (18).

Synthesis of chimeric TP constructs, site-directed mutagenesis, and cell cultures. The wild-type TP, chimeric TP-IP genes carrying the rho-1D4 epitope tag at the C terminus, and specific site-directed mutations were synthesized commercially (GenScript) and incorporated into the plasmid expression vector pMT4 (18–20). The design and analyses of these constructs are described in Results. The genes were transiently expressed in heterologous cell lines, and the membranes were prepared according to previously published protocols (18, 20). To minimize variations in transfection efficiency, the chimeric sequences were codon optimized for their expression in mammalian cells, and equal amounts of DNA (6 μg per 5×10^6 cells) were used. Following the transient transfection, cell viabilities were determined, and viable cells were used for the assays.

Radioligand binding assays. Saturation binding assays were carried out using ^{3}H-labeled SQ 29548 (product no. NET936250UC; PerkinElmer) and as described previously (18).

Determination of receptor expression by flow cytometry analysis. The cell surface expressions of TP, IP, and different constructs were determined using a BD FACSCanto flow cytometer. HEK293T cells were transfected with 6 μg of DNA per 5×10^6 cells using Lipofectamine 2000. Twenty-four hours after the transfections, 1×10^5 viable cells were taken into a flow cytometry tube and washed 2 to 3 times with fluorescence-activated cell sorter (FACS) buffer (phosphate-buffered saline [pH 7.4] containing 0.5% bovine serum albumin) by centrifugation for 4 min at 1,500 rpm. The cells were incubated for 60 min on ice with a 1:100 dilution of the polyclonal antibody $TBXA_2R$ (0.5 mg/ml) (catalog no. LS-B4842; LifeSpan BioSciences) and IP antibody (item no. 10005518; Cayman Chemicals), which target the N termini of the human TP and IP, respectively. The cells were washed 2 to 3 times with FACS buffer and incubated in the dark with a 1:500 dilution of the secondary antibody Alexa Fluor 488 for 60 min on ice. The cells were washed 2 to 3 times with FACS buffer and resuspended in 200 μl of FACS buffer. The fluorescence signals of 1×10^4 cells/tube were measured using single-color analysis by the BD FACSCanto analyzer using settings of 159 V for forward scatter (FSC), 379 V for side scatter (SSC), and 385 V for Alexa Fluor 488. The results were analyzed using the FACSDiva and FlowJo software programs. The cell surface receptor expression was calculated as a percentage of the wild-type TP expression level, which was set to 100%. The nonspecific signal from mock-transfected cells was 10% ± 2%.

Determination of intracellular cAMP. The cAMP assays were carried out in HEK293S cells using a commercially available cAMP assay kit (HitHunter cAMP XS+; DiscoveRx, Fremont, CA) and as described previously (19). In brief, 48 h after transient transfection, the cells were stimulated with various concentrations (from 10^{-6} M to 10^{-12} M) of the agonist iloprost for the IP (positive control) and the agonist U46619 for the TP and chimeric TP-IP receptors. Luminescence was measured after overnight incubation using a FlexStation 3 microplate reader (Molecular Devices, CA). The assays were carried out 3 to 5 times each in duplicate, and the data were analyzed using PRISM software version 5 (GraphPad Software Inc., San Diego, CA). The cAMP values of the chimeric TP-IP receptors, expressed in relative luminescence units (RLUs), were normalized to that of the WT IP.

Determination of intracellular IP_3 and calcium. The changes in intracellular calcium levels were measured by using the fluorescent calcium-sensitive dye Fluo-4NW (Invitrogen) and as described previously (18). Receptor activation was determined by measuring the changes in intracellular calcium levels after the application of different concentrations of the agonist U46619 for the TP and chimeric TP-IP receptors and of iloprost for IP receptors using a FlexStation-3 fluorescence microplate reader (Molecular Devices, CA) at 525 nm, following excitation at 494 nm. Dose-response curves were generated and 50% effective concentrations (EC_{50}s) were calculated by nonlinear regression analysis using PRISM software version 5.0 (GraphPad Software Inc., San Diego, CA) after subtracting the responses of mock-transfected cells that were stimulated with the same concentrations of the agonists. For an estimation of the calcium that was mobilized using the nonratiometric calcium indicator dye Fluo-4NW, we used the $\Delta F/F$ ratio, which calculates approximate calcium levels using the equation $\Delta F/F = (F - F_{base})/(F_{base} - B)$, where F is the measured fluorescence intensity of Fluo-4NW, F_{base} is the fluorescence intensity of Fluo-4NW in the cell before stimulation, and B is the background signal determined from areas adjacent to the cell (21). The inositol-1,4,5-trisphosphate (IP_3) assays were carried out in HEK293T cells using a commercially available IP_3 assay kit (HitHunter IP_3 fluorescence polarization [FP] assay; DiscoveRx, Fremont, CA) according to the instructions supplied by the manufacturer. The assay details are provided in the supplemental material.

Statistical analysis. Statistical analyses using one-way analysis of variance (ANOVA) with Tukey's *post hoc* test from at least 3 independent experiments (performed in duplicate) were done to determine which chimeric receptor or mutant exhibited a response that was statistically different from that of the wild-type TP or IP, with a P value of <0.05 considered to be statistically significant (Table 1; see Fig. 4) (see also Fig. S3 and S5 in the supplemental material).

Immunofluorescence analyses. HEK293T cells were seeded into six-well tissue culture plates containing glass coverslips treated with sterilized poly-L-lysine (Sigma). The cells were transiently transfected with the wild-type TP or the chimeric receptors using Lipofectamine 2000. The procedure was similar to previously published protocols (22). Representative cells were visualized using an Olympus IX81 microscope for cytoplasmic or plasma membrane localization of the receptors.

Protein molecular modeling. We have used the homology model of the TP alpha isoform (TPα) that was built and validated by our group previously (18). The chimeric receptors TP ICL1-IP, TP ICL2-IP, TP ICL2B-IP, TP ICL3B-IP, and TP ICL3C-IP were also modeled and docked with the TP agonist ligand U46619 following a published protocol (18).

TABLE 1 Summary of ligand binding properties and expressions of the wild-type TP, IP, and chimeric receptors

Receptor	Intracellular loop(s)	K_d[a,b] (nM)	B_{max}[a,c] (pmol/mg)	Cell surface[d] expression (%)	EC_{50}[e] Ca^{2+} (nM)	EC_{50}[f] cAMP (nM)
Wild-type TP		5.8 ± 1.3	5.1 ± 0.3	100	13.1 ± 0.8	ND
Wild-type IP				108 ± 1	ND	7.7 ± 0.3
TP ICL1-IP	ICL1	4.8 ± 1.1	8.9 ± 0.4	96 ± 7	4.6 ± 1.1	ND
TP ICL2-IP[g]	ICL2	ND		93 ± 7	8.3 ± 0.5	22.7 ± 0.3
TP ICL2A-IP	ICL2	4.3 ± 0.6	3.1 ± 0.3	76 ± 6	11.0 ± 0.4	51.2 ± 1.3
TP ICL2B-IP	ICL2	5.3 ± 0.8	9.3 ± 0.4	108 ± 7	15.6 ± 2.0	62.2 ± 1.2
TP ICL3-IP[g]	ICL3	ND		42 ± 4		
TP ICL3A-IP	ICL3	ND		49 ± 7		
TP ICL3B-IP[g]	ICL3	ND		92 ± 2	32.4 ± 1.3	39.8 ± 1.1
TP ICL3C-IP	ICL3	5.8 ± 1.2	3.4 ± 0.4	89 ± 1	61.6 ± 2.1	ND
TP ICL2B-ICL3B–IP	ICL2/3	8.1 ± 3.9	0.9 ± 0.2	97 ± 2	30.7 ± 0.2	18.3 ± 0.2
TP ICL2B-ΔYLYAQ[h]	ICL2	7.7 ± 4.0	0.7 ± 0.2	81 ± 9	37.5 ± 0.2	ND
R60L	ICL1	9.8 ± 1.3	1.3 ± 0.2	85 ± 2	44.9 ± 0.4	
TP ICL2B-R60L	ICL1/2	19.7 ± 2.0	2.5 ± 0.2	96 ± 2	12.1 ± 0.4	
TP ICL2B-3B–IP–R60L	ICL1/2/3	21.7 ± 3.9	4.1 ± 0.2	92 ± 1	17.0 ± 0.2	
T135A	ICL2	7.6 ± 2.6	5.7 ± 0.8	72 ± 12	ND	
R136A	ICL2	8.7 ± 1.9	5.5 ± 0.5	81 ± 17	14.2 ± 0.4	
R147A	ICL2	9.2 ± 2.3	6.0 ± 0.6	82 ± 17	ND	
R148A	ICL2	7.3 ± 2.1	9.8 ± 0.1	46 ± 12	12.2 ± 0.3	
H224A[g]	ICL3	ND		49 ± 10		
V225A[g]	ICL3	ND		88 ± 8		
E230A[g]	ICL3	ND		72 ± 2	8.0 ± 0.2	
Q252A[g]	ICL3	ND		97 ± 19	2.1 ± 0.2	

[a] The values are expressed as the mean ± standard error (SE) of 3 to 5 experiments in duplicate performed using the TP antagonist ^{3}H-labeled SQ 29548 as the radioligand (product no. NET936250UC, PerkinElmer). ND, not determined.
[b] K_d, affinity of the antagonist SQ 29548 for the receptor.
[c] B_{max}, binding maximum of the ligand SQ 29548 for the receptor, expressed as pmol of the TP receptor per mg of total membrane protein.
[d] Cell surface expression of the receptor determined using flow cytometry (see Materials and Methods), represented using the wild-type TP set at 100%.
[e] EC_{50}s in this column indicate the molar concentrations of the agonist U46619 that produce 50% of the maximal possible effect (calcium mobilization) for the TP and chimeric or mutant receptors. A one-way ANOVA of the EC_{50} values for calcium mobilized between the wild-type TP and the chimeric receptors and mutants showed a significant difference ($P < 0.05$).
[f] EC_{50}s in this column indicate the molar concentrations of the agonist iloprost for IP and of U46619 for the TP and chimeric or mutant receptors that produce 50% of the maximal possible effect (cAMP production).
[g] No significant specific binding to the antagonist ^{3}H-labeled SQ 29548 and/or dose-dependent response to the agonist for these receptors was detected under our assay conditions.
[h] TP ICL2B-IP with the YLYAQ sequence in the middle of ICL2B removed.

Receptor-Gα peptide docking. The active conformation of the TP receptor was docked with the 14 C-terminal amino acids of human Gαq (GenBank accession no. AAB39498.1). The 14 C-terminal amino acids of the human Gαq were modeled using rat Gαq (3AH8) as a template. The receptor and Gα peptide were docked using the ZDOCK server (23). The docking calculations were carried out using the fast Fourier transform-based protein-docking method using ZDOCK. It involves searches of all possible binding modes in the translational and rotational spaces between two proteins and evaluates each using an energy-scoring function (24). The poses with the best energy scores were chosen for further analysis. Our docking studies revealed that the 14-amino-acid Gα peptide bound to the TP in two positions, one between ICL1 and ICL2 and the other between ICL2 and ICL3. To determine which of the two positions was the correct one, we utilized the recently solved structure of the β_2 adrenergic receptor (β_2AR)-Gαs (3SN6) protein complex. We built the human Gαq (35 to 359 residues) model by homology modeling using the mouse Gαq (2RGN) crystal structure as a template, and using the TP model from above, both were threaded on the β_2AR-Gαs (3SN6) complex. Molecular dynamic simulations (10 ns) using the Tripos force field were performed on the TP-Gαq complex using the SYBYL-X v2.1 molecular modeling suite (Tripos Inc.). In this model, the C-terminal region of Gαq was located between the ICL2 and ICL3 of the TP. Based on this, the model with the C-terminal Gαq peptide bound between ICL2 and ICL3 of the TP was used for further analysis, and the models were visualized using PyMOL.

RESULTS

Design and construction of chimeric TP-IP receptors. The amino acid sequences of the TP and IP receptors were obtained from the G protein-coupled receptor database (GPCRDB), and alignment was performed using ClustalW (25, 26). From the multiple-sequence alignment, the TP chimeras containing intracellular IP loops were designed in three steps. In the first step, TM sequence prediction servers were used in predicting the TM regions (see Table S1 in the supplemental material). In the second step, a total of four chimeric TP-IP receptors were designed as follows: three TP chimeric receptors were constructed containing each of the three ICLs of the IP and the other one (TP-ICL1,2,3-IP) with all the loops replaced (Fig. 1A). In the final step, the sequential replacement of ICL2 and ICL3 of the TP with the IP sequence was carried out by replacing six amino acids at a time (i.e., three amino acids from the N termini and three amino acids from the C termini of the loop regions). Following the procedure described above, two ICL2 chimeric receptors, TP ICL2A-IP and TP ICL2B-IP, and three chimeric receptors, TP ICL3A-IP, TP ICL3B-IP, and TP ICL3C-IP, were constructed for ICL3 (Fig. 1B).

Effect of loop replacements on TP expression, antagonist binding, and internalization. The levels of functional receptor

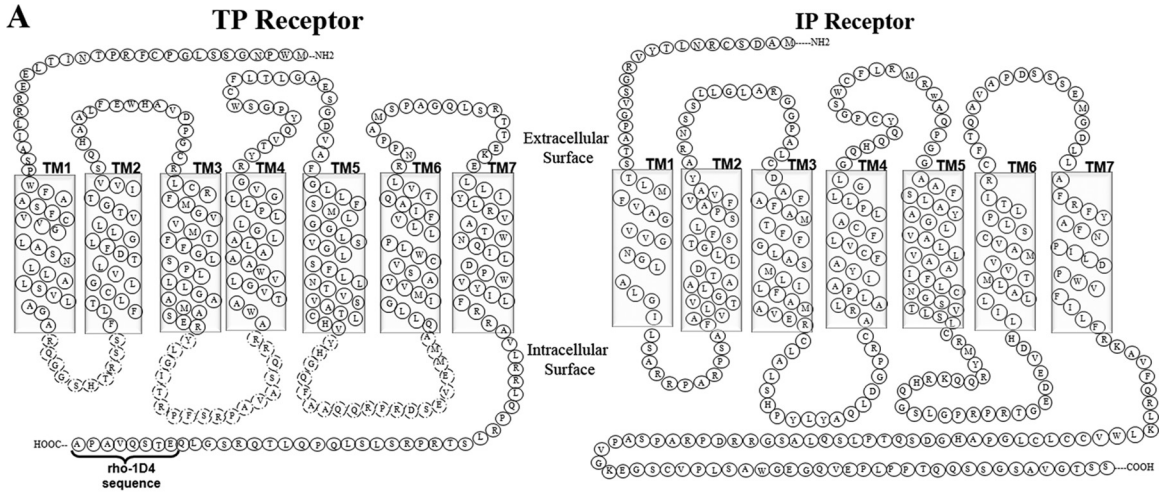

FIG 1 Schematic representation of the amino acid sequence of the TP, IP, and chimeric receptors. (A) Secondary structure representation of the TP and IP amino acid sequences. The intracellular loop (ICL) regions replaced in the TP are indicated by dashed lines. (B) The amino acid sequences of the TP replaced by the IP sequence are underlined. TP ICL1-IP represents the TP with its first ICL replaced by the IP ICL1. Similarly, TP ICL2-IP represents the TP with its second ICL replaced by the IP ICL2; TP ICL3-IP represents the TP with its third ICL replaced by the IP ICL3; TP ICL2B-ΔYLYAQ-IP represents the TP ICL2B-IP receptor with the pentapeptide YLYAQ sequence deleted.

expression were quantified by saturation ligand binding assays on the WT TP and the chimeric receptors expressed in COS-1 cells using the radiolabeled TP antagonist SQ 29548 (Table 1; see also Fig. S1 in the supplemental material). Among the complete loop replacements, only the TP ICL1-IP receptor with the replacement of ICL1 of the TP with that of the IP bound to the antagonist with a dissociation constant (K_d) of 4.8 ± 1.1 nM, which is close to the K_d of 5.8 ± 1.3 nM for the WT TP. However, the complete replacement of ICL2 and ICL3 of the TP with IP ICLs failed to show any specific binding to SQ 29548 (see Fig. S1 in the supplemental material). To elucidate whether this loss in antagonist binding was due to major structural changes in the receptor that perturb the ligand binding pocket or due to poor cell surface expression and/or misfolding of the receptor, analyses of receptor expression by FACS, Western blotting, and immunofluorescence microscopy were carried out on these chimeric receptors. The WT TP, IP, and the chimeric constructs, with the exception of the TP ICL3-IP and TP ICL3A-IP chimeras, were expressed at similar levels based on FACS analyses (Table 1). Immunofluorescence analyses showed TP ICL3-IP and TP ICL3A-IP to be partly retained in the intracellular compartments (see Fig. S2A in the supplemental material). The functional receptor expression observed with the saturation radioligand binding, cell surface receptor expression by FACS analysis, and cellular localization by immunofluorescence were further supported by Western analysis (see Fig. S2B in the supplemental material).

The ICL2 chimeric receptors TP ICL2A-IP and TP ICL2B-IP bound to the antagonist with affinities similar to that of the WT TP, but TP ICL2B-IP showed a 2-fold-higher B_{max} (binding maximum of the ligand SQ 29548) than that of the WT TP (Table 1). In comparison, among the ICL3 chimeric receptors, only TP ICL3C-IP, with the shortest amino acid replacement, showed specific binding to the TP antagonist SQ 29548. Interestingly, the TP ICL3B-IP chimeric receptor showed no significant specific binding to SQ 29548 (Table 1). The chimeric receptor with all three TP ICLs replaced with IP ICLs failed to show any specific binding to SQ 29548, and immunofluorescence analyses showed that a majority of the receptors expressed were not targeted to the cell surface and were retained in the intracellular milieu (data not shown).

To elucidate whether any of the chimeric receptors undergo internalization in the absence or presence of an agonist, the TP and the chimeras were treated with the agonist U46619, while the IP was treated with its agonist, iloprost. Interestingly, the TP and the chimeric receptors did not show any significant agonist-dependent or -independent internalization, whereas the IP showed a significant agonist-dependent internalization, with only ~40% of the receptor on the cell surface (see Fig. S2C in the supplemental material).

Characterization of intracellular Ca^{2+} signaling of chimeric receptors. The characterizations of Gαq-mediated signaling of the WT TP and chimeric receptors were carried out by measuring the intracellular Ca^{2+} flux upon stimulation with the agonist U46619 (Fig. 2). Interestingly, the TP ICL1-IP chimeric receptor with the complete replacement of ICL1 of TP with IP showed an increase in U46619 potency (a decrease in the EC_{50} for half-maximum response), with an EC_{50} of 5 nM compared to an EC_{50} of 13 nM for the WT TP (Table 1). The TP ICL2-IP chimeras showed a left shift in dose response (Fig. 2), with the restoration in EC_{50}s to wild-type TP levels, as the TP sequence increased in the ICL2

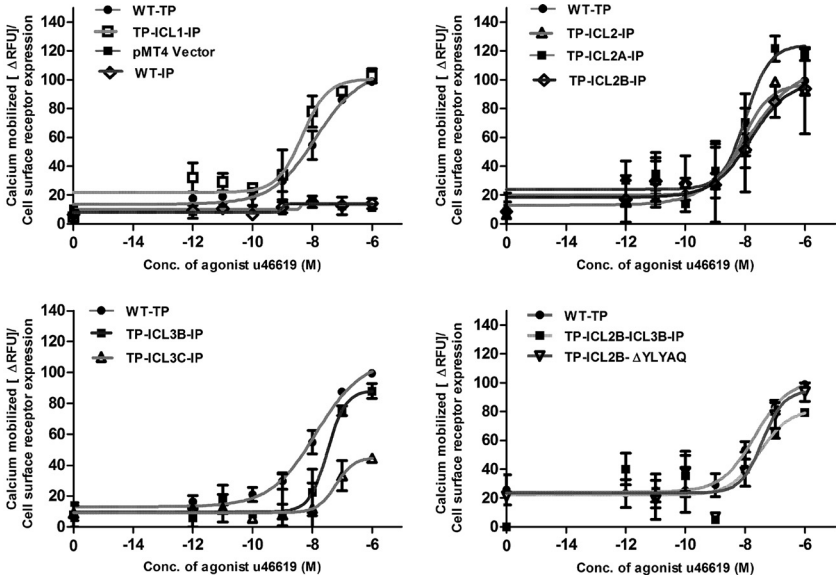

FIG 2 Characterization of Gαq-mediated signaling of the wild-type TP and chimeric receptors. Receptor activity was determined by measuring the agonist-independent and -dependent changes in intracellular calcium levels using transiently transfected HEK293T cells. The data show the basal (zero concentration of agonist or water alone) and agonist U46619-induced calcium mobilization for the WT TP, chimeric receptors, and mock-transfected (vector pMT4) HEK293T cells. The results are expressed as a percentage of the WT TP activity and are from at least three independent experiments performed in duplicate. The results were normalized to calcium mobilized (ΔRFUs) relative to cell surface expression of the receptors as determined by FACS.

region (Table 1). The TP ICL3-IP and TP ICL3A-IP chimeric receptors did not show any dose-dependent increases in intracellular Ca^{2+} (data not shown); this is in agreement with our expression data, which showed that a majority of these two chimeras were retained in the intracellular milieu. The TP ICL3B-IP, with an intermediate amount of amino acids replaced, and TP ICL3C-IP, with the least number of amino acids replaced, showed intracellular Ca^{2+} mobilizations equivalent to ~70% and ~25% of the TP-generated signals, with EC_{50}s of 32 nM and 61 nM, respectively (Fig. 2).

Characterization of intracellular cAMP signaling of chimeric receptors. To determine whether the chimeric TP-IP receptors can couple to Gαs and stimulate cAMP production, we analyzed the chimeric receptors for their ability to generate cAMP upon stimulation with the TP agonist U46619 (Fig. 3). The WT IP activated by its agonist iloprost was used as a positive control, and the WT TP stimulated with U46619 was used as a negative control (Fig. 3A). The WT TP, TP ICL1-IP, and all the TP ICL3-IP chimeras, except TP ICL3B-IP, did not generate any dose-dependent cAMP response upon stimulation with the agonist U46619 (Fig. 3). In contrast, all the TP ICL2 chimeras with complete and sequential replacements of the amino acids of ICL2 showed Gαs-mediated cAMP signaling (Fig. 3B). Among the ICL3 chimeras, only TP ICL3B-IP with an intermediate number of amino acids replaced showed an agonist concentration-dependent increase in cAMP signaling (Fig. 3).

Characterization of the intrinsic and basal signaling of the chimeric receptors. Both intracellular Ca^{2+} and cAMP assays were carried out with the receptors stimulated with water alone to determine the basal or agonist-independent signals and with a single saturating concentration (1 μM) of agonists to determine the maximum agonist-induced or intrinsic signals (Fig. 4). The complete loop replacement chimeras, TP ICL1-IP and TP ICL2-IP, and the ICL2 and ICL3 chimeras TP ICL2A-IP, TP ICL2B-IP, and TP ICL3B-IP showed intrinsic activities for intracellular Ca^{2+} that were 60% to 90% of that of the WT TP (Fig. 4A). To obtain more direct evidence of phospholipase Cβ (PLCβ) activation, agonist-stimulated IP_3 generation was measured (see Fig. S3 in the supplemental material). The levels of intrinsic activity obtained with the IP_3 assay were similar to those observed for intracellular Ca^{2+}. Interestingly, the TP ICL2A-IP and TP ICL2B-IP chimeric receptors showed constitutive IP_3 and Ca^{2+} signaling to various degrees (see Fig. S3 and S4A in the supplemental material).

Surprisingly, the TP ICL3B-IP and TP ICL2A-IP chimeric receptors showed U46619-induced cAMP signaling equivalent to that of the WT IP-generated signal (IP stimulated with iloprost) (Fig. 4B). Only the TP ICL1-IP and TP ICL3C-IP chimeric receptors showed reduced cAMP signaling.

Protein molecular modeling. Previous studies have shown that there are multiple regions on the Gα subunit that are involved in mediating GPCR-G protein interactions (27, 28). Recent mutational studies indicated that the α4-β6 loop of Gαq is important, while structural studies have shown that the carboxy-terminal residues, including the α4-5 helix and the αN-β1 junction of the Gαs subunit, are important in mediating GPCR-G protein coupling (29, 30).

Molecular models of the TP and the chimeric receptors bound to the agonist U46619 and docked with the 14 C-terminal amino acids of human Gαq (GenBank accession no. AAB39498.1) were constructed to interpret the results in structural terms. The intermolecular interactions between the TP chimeric models and Gα peptide sequence are listed in Table S2 in the supplemental material. Docking simulations between the TP ICL2B-IP chimeric receptor and the Gα C-terminal sequence revealed a series of H-bonding and hydrophobic interactions that differed from those of TP ICL2 (Fig. 5). In the WT TP model, $Glu129^{3.49}$ from the con-

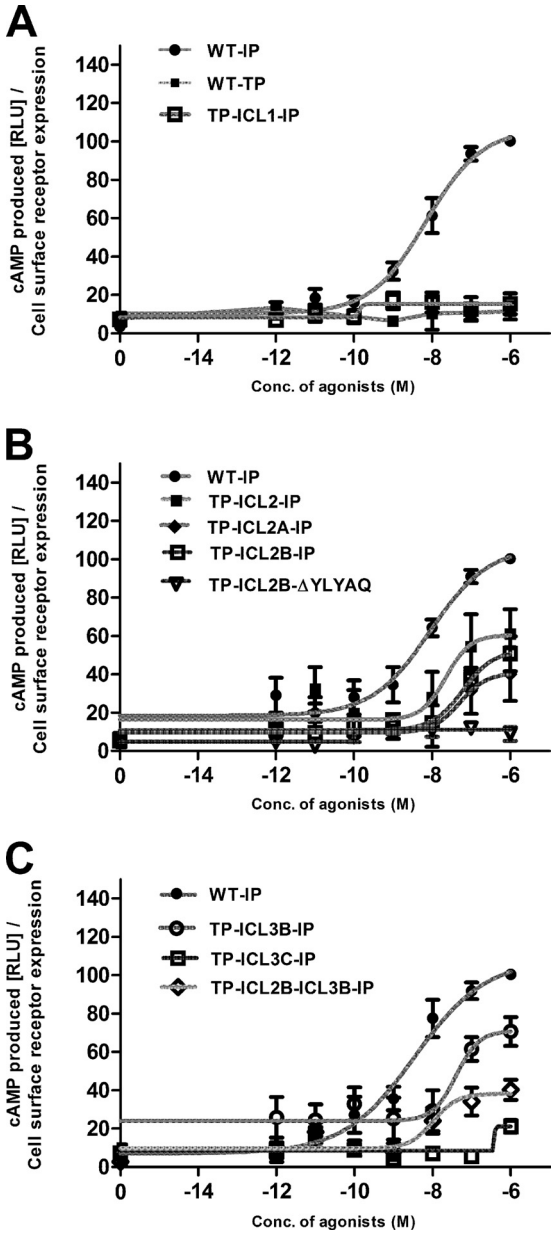

FIG 3 Agonist-induced cAMP production by the IP, TP, and TP-IP chimeric receptors. Receptor activity was assessed by measuring the cAMP produced in a dose-dependent manner by the receptors expressed in HEK293S cells as described in Materials and Methods. (A) Basal (zero concentration) and agonist (U46619 or iloprost)-induced cAMP production for the WT IP, WT TP, and TP ICL1-IP chimeric receptors. The WT IP and ICL2 chimeric receptors (B) and the WT IP and ICL3 chimeric receptors (C) are shown. The cAMP values of the chimeric TP-IP receptors, measured in relative luminescence units (RLUs), are expressed as a percentage of the WT IP activity and are from at least three independent experiments performed in duplicate. The results were normalized to cAMP produced (RLUs) relative to cell surface expression of the receptors as determined by FACS.

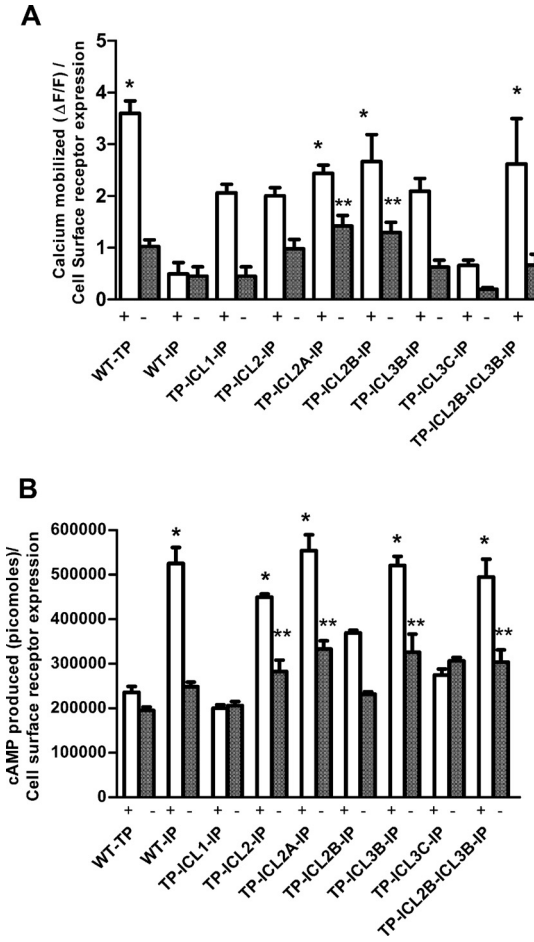

FIG 4 Bar plot representation of the calcium mobilized (A) and cAMP produced (B) upon activation of the TP or IP and chimeric receptors. The cells expressing the IP were stimulated with the IP agonist iloprost, while cells expressing the TP and TP-IP chimeras were stimulated with the TP agonist U46619. Shown are the agonist-independent or basal activities (−) and the activities after stimulation (+) with a single saturating concentration (1 μM) of agonists to determine the maximal agonist-induced or intrinsic signals. The results were normalized to the amounts of calcium mobilized and cAMP produced relative to cell surface expression of the receptors as determined by FACS. The results are from a minimum of 3 independent experiments performed in duplicate. A one-way ANOVA with Tukey's *post hoc* test was used to check the significance levels of the amounts of calcium mobilized or cAMP produced. The single asterisks indicate a significant difference in the amount of cAMP produced or calcium mobilized at the highest concentration of agonist with respect to the WT TP (for cAMP produced) or WT IP (for calcium mobilized) ($P < 0.05$). The double asterisks indicate calcium mobilization at a basal level compared to WT IP basal level activity and cAMP produced at a basal level compared to WT TP basal activity ($P < 0.05$). The bar plots do not include the chimeras TP ICL3-IP and TP ICL3A-IP, as they failed to show any dose-dependent response. The error bars represent means ± standard deviation (SD).

served E(D)RY motif on TM3 is involved in a salt bridge with Arg148 of ICL2, possibly restraining the ICL2 loop in an inactive conformation. In addition, there is a network of hydrogen bonds involving Glu355 and Tyr356 from the Gαq peptide and Thr135 and Arg136 from TP ICL2. In the TP ICL2B-IP chimeric model, the salt bridge is missing, and new H-bond interactions involving Arg136 on ICL2B, Glu230 on ICL3 with Glu355, and Lys354 of the Gα peptide were observed. TP ICL2B-IP differs from the WT TP in the absence of pentapeptide FSRPA sequence in the middle of the ICL2 loop (Fig. 1). This sequence is replaced by another pentapeptide sequence, YLYAQ, in the TP ICL2B-IP chimera. To elucidate whether the presence of the YLYAQ sequence or the absence of the FSRPA sequence is responsible for the TP ICL2B-IP

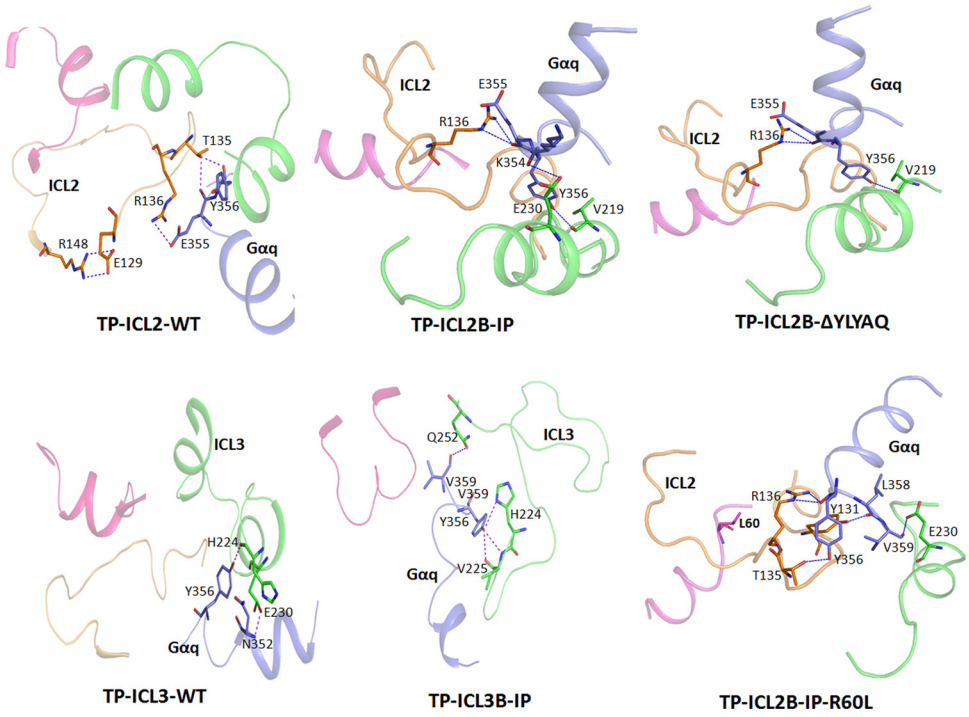

FIG 5 Molecular models of the TP and TP-IP chimeric receptors bound to the Gα C-terminal peptide. The residues involved in the interactions are represented as sticks; hydrogen bonds are shown as blue lines. The color representations of the different ICLs are as follows: ICL1, magenta; ICL2, light orange; ICL3, green; and Gα peptide, blue. For clarity, only the intracellular loops (ICLs) are shown. The interactions observed in TP ICL2-WT and TP ICL3-WT and the chimeric TP ICL2B-IP, TP ICL2B-IP-R60L, TP ICL2B-ΔYLYAQ-IP, and TP ICL3B-IP receptors bound to Gα peptide are shown. In the TP ICL2B-IP-R60L model, Leu60 on ICL1 is pointing away from the Gα peptide binding region located between ICL2 and ICL3. Note the loss of the secondary structure in ICL3 of the TP ICL3B-IP chimera compared to the wild-type TP ICL3.

phenotype, molecular models of the TP-Gα peptide complex with the FSRPA sequence removed and TP ICL2B-IP-Gα peptide complex with the YLYAQ sequence removed were analyzed. Removing the FSRPA sequence from docking simulations in the WT TP revealed no major changes (Fig. 5).

The Gα peptide-bound TP ICL3-IP chimeric receptors revealed fewer H-bond and hydrophobic interactions than the TP ICL2-IP chimeric receptors (Fig. 5). In the TP ICL3B-IP model, we observed interactions involving His224 and Val225 at the cytoplasmic end of TM5 and Glu230 and Gln251 on TP ICL3B-IP with the Tyr356 and Val358 on the Gα peptide sequence. Interestingly, a triad of hydrogen bonds connected the side chain −OH of Tyr356 with the amide of His224 and backbone of Val225. Another interesting feature is the extensive loss of secondary structure in ICL3 of the TP ICL3B-IP chimeric receptor compared to that of the WT TP (Fig. 5).

Amino acid replacements guided by molecular modeling. To validate the predictions from our molecular models, amino acids and loop regions that were shown by the models to be important for receptor activation and/or Gα peptide binding were replaced, and the mutants were characterized. Molecular models indicated that the YLYAQ sequence of TP ICL2B-IP was important in determining the G protein specificity of the TP. Therefore, a TP ICL2B-IP receptor with the pentapeptide YLYAQ sequence deleted (TP ICL2B-ΔYLYAQ-IP) was constructed and characterized (Table 1). In addition, the residues Thr135, Arg136, Arg147, and Arg148 on TP ICL2B-IP and His224, Val225, Glu230, and Gln252 on TP ICL3B-IP were replaced with alanine, and the mutants were characterized (Table 1).

The functional characterization of the TP ICL2B-ΔYLYAQ-IP chimeric receptor revealed that it is expressed at a lower level, compared to WT TP, as shown by both the B_{max} and FACS analysis, but it has an affinity toward the TP antagonist SQ 29548 that is similar to that of the WT TP (Table 1). Though it displayed a small right shift in the U46619 dose response with an EC_{50} of 37 nM (Fig. 2), as expected, this chimeric receptor did not generate cAMP upon stimulation with the TP agonist U46619 (Fig. 3). This validates our molecular model and revealed that the YLYAQ amino acid sequence in ICL2 is responsible for the Gαs-coupling specificity of the TP ICL2B-IP chimeric receptor.

Since the TP ICL2B-IP and TP ICL3B-IP chimeric receptors have intermediate IP ICL2 and ICL3 sequence lengths and showed 60% and 100%, respectively, of cAMP generation upon stimulation with the TP agonist, we wanted to test whether combining these two loops (ICL2B and ICL3B) in one chimeric construct would result in a super chimera. Therefore, the chimeric TP ICL2B-ICL3B–IP receptor was constructed and analyzed. This chimeric receptor showed good intrinsic Ca^{2+} mobilization (~90%) and cAMP production, indicating that there is a cumulative effect upon adding two loops, ICL2B and ICL3B (Fig. 4).

The R148A mutant on ICL2 was expressed at low levels but showed hyperactivity with a large upward shift in the U46619 dose response (see Fig. S4 in the supplemental material). This shows that Arg148 in ICL2 restrains the activity of the receptor, by either forming a salt bridge with Glu129, as in the WT TP model, or being a major contributor to the H-bond network, as observed in the TP ICL2B-IP chimeric receptor. The R136A mutant behaved like the WT TP in its ligand binding properties (see Fig. S4 in the

supplemental material) but showed a slightly elevated level of basal Ca^{2+} signaling (see Fig. S5 in the supplemental material). The T135A and R147A mutants both bound to the antagonist SQ 29548, but R147A showed a reduced affinity toward the antagonist and twice the basal Ca^{2+} signaling of either the WT TP or the WT IP (Table 1; see also Fig. S5 in the supplemental material). This result shows that the H-bonding capabilities of Thr135, Arg136, and Arg147 are crucial for Gαq coupling, while Arg148, through its interaction with the ERY motif on TM3, is important for receptor activation.

Natural variants in the intracellular loops and predicting their roles using chimeric receptors. To test the stringencies of our molecular models and chimeric constructs, we introduced naturally occurring polymorphic variants into select chimeric constructs. Currently, there are two known signaling-deficient genetic variants in the TP and IP within the ICL regions: the TP R60L variant present in the ICL1 and the IP R212C variant (by amino acid sequence analysis, Arg212 in the IP corresponds to His224 in the TP) (see Fig. S6 in the supplemental material) in ICL3, which was recently shown to cause cardiovascular disease progression (31). Molecular modeling studies revealed Arg60 in TP to interact with Met126 and Arg130 of the ERY motif on TM3 through hydrogen-bond interactions (see Fig. S7 in the supplemental material). In addition, the salt bridge between Glu129 of the ERY motif on TM3 and Arg148 was also present. Interestingly, the introduction of R60L in the TP led to the disappearance of interactions with Met126 and Arg130, but the Glu129 and Arg148 interaction was found to be intact. However, in the case of TP ICL2B-IP-R60L, the interactions between Met126 and Arg130, as well as salt bridge interactions between Glu129 and Arg148, were absent, mimicking a more active conformation. As predicted from the molecular models, the functional characterization of the TP ICL2B-IP-R60L and TP ICL2B-ICL3B–IP–R60L chimeras showed that both were able to rescue the Ca^{2+} mobilization of the signaling-deficient R60L to wild-type TP levels (Table 1; see also Fig. S4 in the supplemental material).

The molecular model of the TP ICL3B-IP receptor predicted interactions involving His224 (which corresponds to Arg212 in the IP) and Val225 at the boundary of TM5 and ICL3 and Glu230 and Gln252 on TP ICL3B-IP with Tyr356 and Val359 on the Gα peptide sequence (see Table S2 in the supplemental material). The H224A and V225A mutations were introduced into the TP ICL3B-IP and characterized. As expected, the H224A and V225A mutations caused a complete loss of signaling by the TP ICL3B-IP chimera (Table 1). No specific binding to the antagonist was observed even for the E230A and Q252A mutants, but they showed increased potencies toward the agonist U46619; this was illustrated by a left shift in the dose response (see Fig. S4 in the supplemental material) and with EC_{50}s that were 2- to 3-fold lower than that of the WT TP (Table 1). Surprisingly, both the E230A and Q252A mutants displayed statistically significant increases in agonist-independent activities (see Fig. S5 in the supplemental material).

DISCUSSION

In this work, we utilized a chimeric receptor and molecular modeling-based mutagenesis approach for elucidating the structural basis of prostanoid receptor-G protein interactions. In the prostanoid family of GPCRs, amino acid sequence analyses of ICLs show diversity in both amino acid composition and sequence length (see Fig. S6 in the supplemental material). Interestingly, IP receptors showed a high degree of sequence conservation compared to TP receptors within the ICL1 and ICL2 regions. We have identified the ICL regions on the prostanoid receptors TP and IP, which contribute toward their G protein specificities and lead to well-documented completely opposite pathophysiological effects. The ICL2 region, specifically the pentapeptide YLYAQ sequence in the middle of the ICL2 of IP, plays an important role in determining Gαs specificity. In addition, ICL3 of the IP also has an important role in Gαs coupling, as demonstrated by our TP ICL3B-IP chimeric receptor, while both the ICL2 and ICL3 regions of the TP play important roles in Gαq-effector coupling. Using the ICL2 and ICL3 chimeras, we were able to rescue signaling of the dysfunctional bleeding disorder genetic variant R60L present in ICL1 to the wild-type TP levels.

Chimeric receptor approach for elucidating GPCR structure and function. Since the introduction of chimeric receptors for delineating the domains involved in ligand binding specificity of class A GPCRs by Kobilka et al. (32), their approach has been used successfully on a number of GPCR systems (33). Studies on chimeric α_1/β_2-adrenergic receptors (α_1AR/β_2AR) with the third ICL of the β_2AR replaced with that of the α_1AR demonstrated ligand binding capabilities similar to those of the β_2AR and showed downstream signaling as an α_1AR (34). Among the dopamine receptors, D1 receptors activate adenylyl cyclase, resulting in the production of second messenger cAMP, whereas the D2 receptors inhibit adenylyl cyclase. D1 chimeric receptors with TM6, TM7, and the C terminus replaced with those of the D2 receptors showed enhanced binding of the D2 agonist and inhibited adenyl cyclase (35). Similar results were also obtained with chimeric receptors composed of gonadotropic luteinizing hormone (LH) and follicle-stimulating hormone (FSH) receptors. The N terminus of the FSH receptor replaced with that of the LH receptor resulted in IP_3 production when stimulated with FSH (36). A chemokine receptor (CCR5) has been shown to interact with HIV and play a crucial role in its entry. The chimeric receptors constructed between bacteriorhodopsin and the CCR5 extracellular segments provided specific insights into the regions in CCR5 that confer HIV coreceptor function (37). The uniqueness of the current study lies in our three-pronged approach to elucidate GPCR-G protein interactions in a receptor family that has been shown only recently to play an important role in the development of human cardiovascular disease. First, we constructed and characterized chimeric receptors with complete and sequential replacements of ICL loops. Next, to interpret the results in structural terms, we built molecular models of the chimeric receptors bound to the Gα peptide. Finally, we used mutagenesis to validate the proposed models of prostanoid receptor-G protein interactions.

ICL1. The TP ICL1 has been implicated in both G protein-dependent and -independent signaling. Earlier studies showed that the dominantly inherited bleeding disorder variant R60L impaired calcium signaling (17), and recent studies have shown that ICL1 in the TP couples with and inhibits the large conductance voltage- and calcium-activated potassium channels (MaxiK channels) (38). It has been proposed that this direct interaction with MaxiK channels facilitates the G protein-independent TP to MaxiK transinhibition, which would promote vasoconstriction (38). Interestingly, the results from our studies show that except for a conserved Arg that is present at analogous positions in ICL1 of prostanoid receptors (Arg56 of the TP ICL1-IP construct cor-

responds to Arg45 of the IP or Arg60 in the TP), the remaining part of the TP ICL1 is not important for activation, as the TP ICL1-IP chimeric receptor showed elevated levels of Ca^{2+} in response to treatment with agonist U46619 (Table 1). cAMP accumulation assays to determine whether ICL1 of the IP can signal through Gαs in the TP ICL1-IP failed to show any response when the chimeric receptor was stimulated with the TP agonist, indicating that it may not be crucial for Gαs-mediated effector signaling. Our mutational studies using the genetic variant R60L, and chimeras containing this variant, showed that R60L is important for receptor activation by mediating interactions with the ERY motif in TM3 rather than by binding to G proteins.

ICL2. All the TP ICL2-IP chimeric constructs, except TP ICL2B-ΔYLYAQ-IP, showed agonist U44619-induced cAMP accumulation of more than 60% of that of the wild-type IP induced with iloprost (Fig. 3). The deletion of the pentapeptide YLYAQ sequence from the TP ICL2B-IP receptor drastically reduced the ability of this chimeric receptor to generate Gαs-mediated cAMP signaling from the wild-type IP levels to that of the wild-type TP levels (Fig. 3). Interestingly, the TP ICL2B-ΔYLYAQ-IP receptor showed very good Ca^{2+} mobilization. In general, the ICL2 chimeric receptors showed significant constitutive activity with respect to a Gαq-based assay (Fig. 4), and there was a gradual restoration of Ca^{2+} signaling (EC_{50}s) to the WT TP values, with an increase in the TP sequence in the loop. From a site-directed mutational analysis of the ICL2 region, we were able to identify Thr135, Arg136, and Arg147 as forming hydrogen bonds crucial for Gαq coupling and Arg148 to restrain the receptor activity by forming a salt bridge with Glu129 (of the ERY motif) in TM3.

The involvement of ICL2 in determining Gαs specificity might be a general mechanism of GPCR-G protein interaction, as shown by the recent structure of the β_2AR-Gs protein complex (12). This is the first crystal structure of a GPCR transmembrane signaling unit consisting of an agonist-occupied β_2AR and nucleotide-free Gs heterotrimer, and it revealed extensive interactions between ICL2, TM5, and TM6 of the β_2AR and the N- and C-terminal regions of the Gαs subunit. Even though we have used only the C-terminal Gα peptide for analysis, our data nevertheless dovetail with the published structural data using the Gs heterotrimer on the importance of ICL2 in determining Gαs specificity.

ICL3. The large ICL3 has very low sequence homology among members of the GPCR family, including the prostanoid receptors. It was previously shown in different class A GPCRs that the proper conformation of ICL3 is important for receptor folding (16). Interestingly, the TP ICL3B-IP showed Gαq-dependent intrinsic signaling of up to 70% of that of the WT TP and Gαs-dependent intrinsic signaling similar to that of the WT IP (Fig. 4). Results from molecular modeling showed a loss of secondary structure in ICL3 of the TP ICL3B-IP chimera compared to the wild-type TP ICL3-IP, resulting in increased flexibility and fewer constraints in the ICL3 region, presumably favoring an active state structure and/or enhanced binding with the G protein. The TP ICL3B-IP sequence seems to be the optimum for both Gαq- and Gαs-dependent signaling, as the further reduction of the IP ICL3 sequence, as in TP ICL3C-IP, causes a drop in both cAMP and Ca^{2+} signal levels. Furthermore, the TP ICL3C-IP chimeric receptor regains binding to the TP antagonist SQ 29548 with affinity and expression levels similar to those of the wild-type TP.

Previous site-directed mutational studies of residues at the cytoplasmic end of TM5 and the start of ICL3 in the TP revealed that Cys223 is important for Gαq signaling (16). The studies on the IP have reported that the genetic variant R212C (corresponding to His224 in the TP) displays defective signaling leading to cardiovascular disease progression (31). TP-IP heterodimerization studies have shown that R212C exerts a dominant negative action of the TP-IP heterodimer (39). Interestingly, an H224R mutation in the wild-type TP was shown previously to have normal ligand binding and calcium-signaling characteristics (16). Our studies show that introducing the H224A mutation into the TP ICL3B-IP chimera disrupts the signaling by this chimera, supporting our observation that the hydrogen-bonding capability of His244 is required for Gαq-mediated calcium signaling. Our data from molecular models, validated by site-directed mutational analysis, point to the importance of the hydrogen-bond triad connecting His224 and Val225 with Tyr356 of the Gα peptide.

Interplay between ICL1, ICL2, and ICL3. In our models, the C-terminal Gα peptide bound to the TP at two different sites (see Materials and Methods), one between ICL1 and ICL2 and the other between ICL2 and ICL3. This is predominantly due to the small size of the peptide used in our studies. Based on the recent structural studies of metarhodopsin II that was bound to a peptide (11), the β_2AR-Gs protein complex (12), and our data, the position between ICL2 and ICL3 is more likely the accurate one. It is possible that the ICL1 region binds to some other sequence of the G protein, such as the amino-terminal region, although the recent crystal structure of β_2AR-Gs does not show ICL1 to be involved in G protein binding. In our data, the most interesting changes were observed for the ICL2 and ICL3 regions. The loop region that has the best basal activity and determines the EC_{50} is ICL2, with ICL3B also playing an important role in conferring intrinsic activity. This shows that both ICL2 and ICL3 in the prostanoid receptors are predominantly involved in G protein coupling and signaling. This differs from the β_2AR-Gs structure, which has shown only the ICL2 region to be involved in Gs coupling. This possible discrepancy is because in our studies, we have used entire loop regions, while the β_2AR-Gs structure is missing the ICL3 region between Arg239 and Cys265. A length of 26 amino acids in ICL3 of the β_2AR is disordered in the structure. The absence of ICL3 might be responsible for the enhanced interactions observed between TM5, which is extended by two helical turns on the cytoplasmic side (compared to the inactive β_2AR structure), and the α5 helix at the C-terminal end of Gs in the β_2AR-Gs structure.

In conclusion, delineation of the interacting domains on the prostanoid receptors TP and IP, and their associated G proteins, was achieved by the construction of chimeric signaling molecules. Detailed analyses of the critical regions responsible for the specificities of prostanoid receptor-G protein interactions provide a framework for understanding the fidelity of prostanoid signaling and the creation of novel tools for drug discovery.

ACKNOWLEDGMENTS

This work was supported by an operating grant from the Manitoba Health Research Council and a Discovery grant (RGPIN 356285) (to P.C.) from the Natural Sciences and Engineering Research Council of Canada., an American Heart Association Established Investigator Award and RO1 grants HL074190 and HL115247 (to J.H.), an MMSF/MHRC Dr. F. W. DuVal Clinical Research Professorship (to S.D.), a New Investigator Award from Heart and Stroke Foundation of Canada (to P.C.). an HSFC operating grant to R.P.B., and graduate fellowships from MHRC/MICH to R.C. and UMGF to S.P.P.

We thank Deepak Upreti for help with flow cytometry analysis.

REFERENCES

1. **Fredriksson R, Lagerstrom MC, Lundin LG, Schioth HB.** 2003. The G-protein-coupled receptors in the human genome form five main families. Phylogenetic analysis, paralogon groups, and fingerprints. Mol. Pharmacol. **63**:1256–1272.
2. **Gleim S, Kasza Z, Martin K, Hwa J.** 2009. Prostacyclin receptor/thromboxane receptor interactions and cellular responses in human atherothrombotic disease. Curr. Atheroscler. Rep. **11**:227–235.
3. **Kinsella BT.** 2001. Thromboxane A2 signalling in humans: a "Tail" of two receptors. Biochem. Soc. Trans. **29**:641–654.
4. **Smyth EM, Grosser T, Wang M, Yu Y, FitzGerald GA.** 2009. Prostanoids in health and disease. J. Lipid Res. **50**(Suppl):S423–S428.
5. **Bresalier RS, Sandler RS, Quan H, Bolognese JA, Oxenius B, Horgan K, Lines C, Riddell R, Morton D, Lanas A, Konstam MA, Baron JA.** 2005. Cardiovascular events associated with rofecoxib in a colorectal adenoma chemoprevention trial. N. Engl. J. Med. **352**:1092–1102.
6. **Grosser T, Fries S, FitzGerald GA.** 2006. Biological basis for the cardiovascular consequences of COX-2 inhibition: therapeutic challenges and opportunities. J. Clin. Invest. **116**:4–15.
7. **Warner TD, Mitchell JA.** 2008. COX-2 selectivity alone does not define the cardiovascular risks associated with non-steroidal anti-inflammatory drugs. Lancet **371**:270–273.
8. **Miggin SM, Kinsella BT.** 2002. Investigation of the mechanisms of G protein: effector coupling by the human and mouse prostacyclin receptors. Identification of critical species-dependent differences. J. Biol. Chem. **277**:27053–27064.
9. **Narumiya S, Sugimoto Y, Ushikubi F.** 1999. Prostanoid receptors: structures, properties, and functions. Physiol. Rev. **79**:1193–1226.
10. **Vassaux G, Gaillard D, Ailhaud G, Negrel R.** 1992. Prostacyclin is a specific effector of adipose cell differentiation. Its dual role as a cAMP- and Ca(2+)-elevating agent. J. Biol. Chem. **267**:11092–11097.
11. **Standfuss J, Edwards PC, D'Antona A, Fransen M, Xie G, Oprian DD, Schertler GF.** 2011. The structural basis of agonist-induced activation in constitutively active rhodopsin. Nature **471**:656–660.
12. **Rasmussen SG, DeVree BT, Zou Y, Kruse AC, Chung KY, Kobilka TS, Thian FS, Chae PS, Pardon E, Calinski D, Mathiesen JM, Shah ST, Lyons JA, Caffrey M, Gellman SH, Steyaert J, Skiniotis G, Weis WI, Sunahara RK, Kobilka BK.** 2011. Crystal structure of the β2 adrenergic receptor-Gs protein complex. Nature **477**:549–555.
13. **Geng L, Wu J, So SP, Huang G, Ruan KH.** 2004. Structural and functional characterization of the first intracellular loop of human thromboxane A2 receptor. Arch. Biochem. Biophys. **423**:253–265.
14. **Wu J, Feng M, Ruan KH.** 2008. Assembling NMR structures for the intracellular loops of the human thromboxane A2 receptor: implication of the G protein-coupling pocket. Arch. Biochem. Biophys. **470**:73–82.
15. **Zhou H, Yan F, Yamamoto S, Tai HH.** 1999. Phenylalanine 138 in the second intracellular loop of human thromboxane receptor is critical for receptor-G-protein coupling. Biochem. Biophys. Res. Commun. **264**:171–175.
16. **D'Angelo DD, Eubank JJ, Davis MG, Dorn GW II.** 1996. Mutagenic analysis of platelet thromboxane receptor cysteines. Roles in ligand binding and receptor-effector coupling. J. Biol. Chem. **271**:6233–6240.
17. **Hirata T, Kakizuka A, Ushikubi F, Fuse I, Okuma M, Narumiya S.** 1994. Arg60 to Leu mutation of the human thromboxane A2 receptor in a dominantly inherited bleeding disorder. J. Clin. Invest. **94**:1662–1667.
18. **Chakraborty R, Pydi SP, Gleim S, Dakshinamurti S, Hwa J, Chelikani P.** 2012. Site-directed mutations and the polymorphic variant Ala160Thr in the human thromboxane receptor uncover a structural role for transmembrane helix 4. PLoS One **7**:e29996. doi:10.1371/journal.pone.0029996.
19. **Arakawa M, Chakraborty R, Upadhyaya J, Eilers M, Reeves PJ, Smith SO, Chelikani P.** 2011. Structural and functional roles of small group-conserved amino acids present on helix-H7 in the β(2)-adrenergic receptor. Biochim. Biophys. Acta **1808**:1170–1178.
20. **Chelikani P, Hornak V, Eilers M, Reeves PJ, Smith SO, RajBhandary UL, Khorana HG.** 2007. Role of group-conserved residues in the helical core of beta2-adrenergic receptor. Proc. Natl. Acad. Sci. U. S. A. **104**:7027–7032.
21. **Takahashi A, Camacho P, Lechleiter JD, Herman B.** 1999. Measurement of intracellular calcium. Physiol. Rev. **79**:1089–1125.
22. **Singh N, Pydi SP, Upadhyaya J, Chelikani P.** 2011. Structural basis of activation of bitter taste receptor T2R1 and comparison with class A G-protein-coupled receptors (GPCRs). J. Biol. Chem. **286**:36032–36041.
23. **Chen R, Li L, Weng Z.** 2003. ZDOCK: an initial-stage protein-docking algorithm. Proteins **52**:80–87.
24. **Pierce B, Weng Z.** 2008. A combination of rescoring and refinement significantly improves protein docking performance. Proteins **72**(1):270–279.
25. **Larkin MA, Blackshields G, Brown NP, Chenna R, McGettigan PA, McWilliam H, Valentin F, Wallace IM, Wilm A, Lopez R, Thompson JD, Gibson TJ, Higgins DG.** 2007. Clustal W and Clustal X version 2.0. Bioinformatics **23**:2947–2948.
26. **Vroling B, Sanders M, Baakman C, Borrmann A, Verhoeven S, Klomp J, Oliveira L, de Vlieg J, Vriend G.** 2011. GPCRDB: information system for G protein-coupled receptors. Nucleic Acids Res. **39**:D309–D319.
27. **Cai K, Itoh Y, Khorana HG.** 2001. Mapping of contact sites in complex formation between transducin and light-activated rhodopsin by covalent crosslinking: use of a photoactivatable reagent. Proc. Natl. Acad. Sci. U. S. A. **98**:4877–4882.
28. **Oldham WM, Hamm HE.** 2008. Heterotrimeric G protein activation by G-protein-coupled receptors. Nat. Rev. Mol. Cell Biol. **9**:60–71.
29. **Hu J, Wang Y, Zhang X, Lloyd JR, Li JH, Karpiak J, Costanzi S, Wess J.** 2010. Structural basis of G protein-coupled receptor-G protein interactions. Nat. Chem. Biol. **6**:541–548.
30. **Scheerer P, Park JH, Hildebrand PW, Kim YJ, Krauss N, Choe HW, Hofmann KP, Ernst OP.** 2008. Crystal structure of opsin in its G-protein-interacting conformation. Nature **455**:497–502.
31. **Arehart E, Stitham J, Asselbergs FW, Douville K, MacKenzie T, Fetalvero KM, Gleim S, Kasza Z, Rao Y, Martel L, Segel S, Robb J, Kaplan A, Simons M, Powell RJ, Moore JH, Rimm EB, Martin KA, Hwa J.** 2008. Acceleration of cardiovascular disease by a dysfunctional prostacyclin receptor mutation: potential implications for cyclooxygenase-2 inhibition. Circ. Res. **102**:986–993.
32. **Kobilka BK, Kobilka TS, Daniel K, Regan JW, Caron MG, Lefkowitz RJ.** 1988. Chimeric alpha 2-,beta 2-adrenergic receptors: delineation of domains involved in effector coupling and ligand binding specificity. Science **240**:1310–1316.
33. **Kim JM, Hwa J, Garriga P, Reeves PJ, RajBhandary UL, Khorana HG.** 2005. Light-driven activation of beta 2-adrenergic receptor signaling by a chimeric rhodopsin containing the beta 2-adrenergic receptor cytoplasmic loops. Biochemistry **44**:2284–2292.
34. **Zhao MM, Gaivin RJ, Perez DM.** 1998. The third extracellular loop of the beta2-adrenergic receptor can modulate receptor/G protein affinity. Mol. Pharmacol. **53**:524–529.
35. **MacKenzie RG, Steffey ME, Manelli AM, Pollock NJ, Frail DE.** 1993. A D1/D2 chimeric dopamine receptor mediates a D1 response to a D2-selective agonist. FEBS Lett. **323**:59–62.
36. **Hirsch B, Kudo M, Naro F, Conti M, Hsueh AJW.** 1996. The C-terminal third of the human luteinizing hormone (LH) receptor is important for inositol phosphate release: analysis using chimeric human LH/follicle-stimulating hormone receptors. Mol. Endocrinol. **10**:1127–1137.
37. **Abdulaev NG, Strassmaier TT, Ngo T, Chen R, Luecke H, Oprian DD, Ridge KD.** 2002. Grafting segments from the extracellular surface of CCR5 onto a bacteriorhodopsin transmembrane scaffold confers HIV-1 coreceptor activity. Structure **10**:515–525.
38. **Li M, Tanaka Y, Alioua A, Wu Y, Lu R, Kundu P, Sanchez-Pastor E, Marijic J, Stefani E, Toro L.** 2010. Thromboxane A2 receptor and MaxiK-channel intimate interaction supports channel trans-inhibition independent of G-protein activation. Proc. Natl. Acad. Sci. U. S. A. **107**:19096–19101.
39. **Ibrahim S, Tetruashvily M, Frey AJ, Wilson SJ, Stitham J, Hwa J, Smyth EM.** 2010. Dominant negative actions of human prostacyclin receptor variant through dimerization: implications for cardiovascular disease. Arterioscler. Thromb. Vasc. Biol. **30**:1802–1809.